Scholarship@Western

2-1-2023

The Hunt for Missing Tornadoes: Using Satellite Imagery to Detect and Document Historical Tornado Damage in Canadian Forests

Joanne Kunkel
University of Manitoba

John Hanesiak
University of Manitoba

David Sills
Western University, David.Sills@uwo.ca

The Hunt for Missing Tornadoes: Using Satellite Imagery to Detect and Document Historical Tornado Damage in Canadian Forests

Joanne Kunkel,[a,b] John Hanesiak,[a,c] and David Sills[b]

[a] *Department of Environment and Geography, University of Manitoba, Winnipeg, Manitoba, Canada*
[b] *Northern Tornadoes Project, Faculty of Engineering, Western University, London, Ontario, Canada*
[c] *Centre for Earth Observation Science, University of Manitoba, Winnipeg, Manitoba, Canada*

ABSTRACT: Historical tornado events from 1982 to 2020 were documented within Canada's forested regions using high-resolution satellite imagery. Tornado forest disturbances were identified using a three-step process: 1) detecting, 2) assessing, and 3) dating each event. A grid of 120 km × 120 km boxes was created covering Canada (excluding the extreme north). Of the 484 boxes, 367 were manually searched. Once a long, narrow region of tree damage was detected, it was first cross-referenced with known tornado databases to ensure it was a unique event. Once events were classified as either tornadic or downburst, the coordinates of the start, worst damage, and end locations were documented, as well as the direction of motion, damage indicators, degree of damage, estimated maximum wind speed, and F/EF-scale rating. In total, 231 previously unknown tornadoes were identified. In Ontario, 103 events were discovered, followed by 98 in Quebec, 9 in Manitoba, 6 in Saskatchewan, 9 in Alberta, 5 in British Columbia, and 1 in New Brunswick. The largest number of discovered tornadoes occurred in 2015, and the largest number of strong F2 tornadoes occurred in 2005. Most of the discovered tornadoes occurred in July for both F/EF1 and F/EF2 ratings. Most tornado tracks had widths between 200 and 400 m, and more than 50% of the tornadoes had a pathlength of less than 10 km. Of all the events that were discovered, 125 events could be fully dated, 19 were dated only by month, 41 were dated only by year, and 46 remained undated.

KEYWORDS: Atmosphere; Tornadoes; Climatology

1. Introduction

Knowing the tornado climatology of a region or country is important not only for tornado warning verification but to better understand 1) the true risk of the hazard, 2) the potential associations with local geographic features (e.g., terrain, bodies of water), and 3) the connections to the storm environment over various scales; the last two can contribute to improved prediction. Tornado climatology data are also useful in other sectors such as insurance and municipality planning.

Knowledge of Canada's tornado climatology is improving. However, a gap remains in our current understanding due to the number of tornadoes in Canada being underestimated (Cheng et al. 2013). Using 11 years of lightning data from 1999 to 2009, population density data, along with a national tornado database from 1980 to 2009 (Sills et al. 2012), Cheng et al. (2013) investigated the predictive relationship between cloud-to-ground lightning and tornado occurrence in order to develop a tornado climatology. The results showed that within populated areas, there was no bias in the underestimation of tornado occurrence, which agreed with previous findings of Hage (1988, 1994), King (1997), and Etkin et al. (2001). However, in sparsely populated regions, the probability of tornado occurrence was higher than what was represented in the 30-yr data record, suggesting that tornadoes have been going undetected in many sparsely populated regions across the country (Cheng et al. 2013).

Most of Canada's population is located along the southern border with the United States, leaving large areas that are sparsely populated and/or heavily forested. As a result, severe weather reports are often rare when severe thunderstorms occur in those regions. Thus, it is difficult to assess the tornado climatology and risk (Western University 2021). In these more sparsely populated regions in Canada, a combination of eyewitness reports (although rare), satellite imagery and S-band Doppler radar networks are used to identify potential regions of tornado damage.

The Northern Tornadoes Project (NTP; Western University 2021) has been using high-resolution satellite imagery since 2018 to help identify wind throw events in these lesser-populated areas. This led to an investigation into whether there were also tornadoes missed in these forested regions prior to NTP. Thus, research began in 2019 to find missing historical tornado events within Canada's forested regions using high-resolution satellite imagery. Tornado-induced forest damage is an important data source to ascertain a more accurate representation of Canada's tornado climatology. Damage from tornadoes that are Fujita-/enhanced Fujita-scale 1 (F/EF1) or greater in strength are generally easy to identify using satellite imagery within the forests of Canada since they result in a large group of fallen, snapped, or uprooted trees.

Several studies have investigated the benefits and use of satellite imagery to assess tornado damage. Sayn-Wittgenstein and Wightman (1975) were the first to use satellite remote sensing to assess tornado damage in the boreal forests of Canada using Landsat Multispectral Scanner Imagery. Dyer (1988) was the first to analyze elongated anomalies found within South American

forests by comparing Landsat imagery with aerial photos and used meteorological records to determine that the forest disturbances were caused by tornadoes (Shikhov and Chernokulsky 2018). Yuan et al. (2002) utilized 23.5-m-resolution images from the Indian Remote-Sensing Satellite Linear Imaging Self-Scanning Sensor 3 (IRS-LISS-3) to estimate damage from the 3 May 1999 tornado outbreak in Oklahoma. They found that a change in the normalized difference vegetation index (NDVI) was a useful tool for detecting and analyzing tornado damage, especially in rural localities (Shikhov and Chernokulsky 2018). Jedlovec et al. (2006) and Molthan et al. (2014) used near-real-time MODIS and high-resolution ASTER imagery provided by the NASA Earth Observing System satellites and determined that tornado damage of F1 or greater intensity are likely more evident in forested regions than in terrain such as grassland or low-forested areas (Shikhov and Chernokulsky 2018). Kingfield and de Beurs (2017) used multispectral satellite imagery as well as NDVI and "Tasseled Cap" to assess 17 tornadoes over forest, grassland, and urban terrains. NDVI and Tasseled Cap were found to provide a good approach for identifying damage, especially over forested areas, but are limited in utility due to the seasonal cycle of agricultural areas and infrastructure density over urban landscapes. Chernokulsky and Shikhov (2018) investigated the 1984 Ivanovo (Russia) tornado outbreak; one of the most fatal tornado events in Europe. The authors used Landsat imagery to discover and survey tornado-induced forest disturbances that were previously undocumented. The boundaries of damage were defined by comparing satellite imagery and were then refined using the normalized difference infrared index (NDII). Burow et al. (2020) used high-resolution satellite imagery and NDVI to analyze the 3 March 2019 tornadoes that occurred in the southeast United States. The results suggested that Sentinel imagery could be used to determine the intensity and dynamics of violent tornadoes in agricultural areas. Chernokulsky et al. (2021) developed a new geographic information system (GIS) database for tornadoes in Russia between 1986 and 2017 by analyzing Landsat imagery to analyze forest cover change.

The purpose of this study is to enhance the tornado climatology of Canada by identifying tornadoes missing from the record. To accomplish this goal, high-resolution satellite data, including assessing and dating these historical events using additional datasets such as archived mesoanalysis products, historical radar, and lightning, were used. Identifying more of these past events will lead to a more robust Canadian tornado climatology that is used to study meteorological processes, for tornado verification, and for use in other sectors that assess risk including insurance industries and municipalities. The article is organized by providing a description of data used and analysis methods (section 2), key results that includes an updated tornado climatology with dates of occurrence and estimated tornado intensities (section 3), limitations of the work (section 4), and conclusions (section 5).

2. Data and methodology

a. Tornado identification

Tornado forest disturbances were documented between the years pre-1982 and 2020 using a three-step process: 1) detecting,
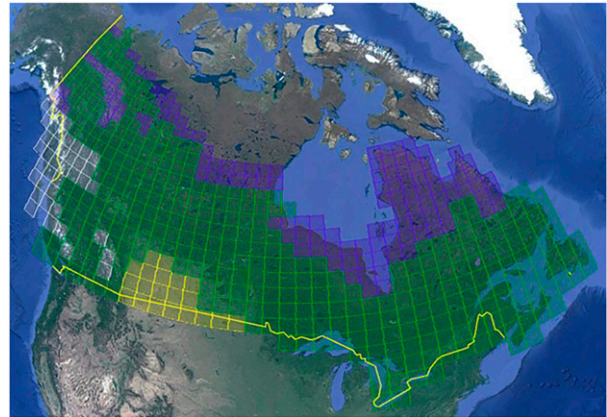

FIG. 1. Map of gridded search regions developed in ArcGIS and overlaid in Google Earth. Green boxes represent regions that were searched. Yellow (agriculture), white (mountainous), and blue (tundra) boxes were not searched because of lack of tree cover (<25%).

2) assessing, and 3) dating each event (when possible). To find the location of past tornadoes, a grid of 120 km × 120 km boxes was created covering most of Canada (excluding the extreme north) to help identify areas that had already been scanned manually, so work was not duplicated (Fig. 1). There were 484 boxes in total. Using 4.7-m monthly mosaicked satellite imagery provided by Planet (http://www.planet.com), 367 of the 484 boxes were manually searched, covering an area of more than 5×10^6 km². Planet's monthly mosaic products are processed to remove cloud cover and haze, and to select images with the best sharpness. Once scenes are selected, they are normalized to a monthly MODIS-based surface reflectance target to minimize inconsistencies between scenes to reduce atmospheric effects (Planet 2021).

According to Bech et al. (2009), as a tornado passes through a forest, it leaves a long and narrow path of damage as trees are snapped and/or uprooted from the ground (Shikhov and Chernokulsky 2018). Over forested regions, tree fall is generally straightforward to detect as it creates noticeable elongated scars, however, over agricultural and treeless northern landscapes, tornado tracks are not as easily detected via satellite imagery. Previous experience with satellite imagery over such terrains led to the conclusion that any historical tornadoes would not be seen in these regions because of the lack of tree cover. The remaining 117 boxes were characterized as primarily agriculture, mountainous, and/or tundra, where tree cover was less than 25% of the 120 km × 120 km box area, and thus were not searched.

The manual tornado search began in September 2019 and ended in May 2021, so the most-recent Planet monthly mosaicked warm-season imagery (August 2019; August 2020) was used for initial track detection once available because the imagery is cloud free. August was chosen since it is later in the tornado season, yet foliage is still green. September is too late in the season because foliage change can appear similar to tree damage. It is ideal to search during peak greenness. Google Earth historical satellite imagery, which has a

TABLE 1. Summary of the satellite imagery products used to detect and date historical tornado events.

	Resolution of imagery used (m)	Dates of available imagery used	Product use	Pros	Cons
Planet daily	3.7	2009–20	Tornado dating	Highest resolution; easy-to-use platform; daily imagery available	Cloud cover; sporadic imagery prior to 2016; expensive
Planet monthly mosaic	4.7	2016–20	Tornado detection	High resolution; easy to use platform; no cloud cover	Lower resolution relative to Planet daily; expensive
Google Earth historical	10–60	1984–2020	Tornado detection	Moderate resolution; free; easy-to-use platform	Yearly imagery only; limited zoom
Land Viewer (Landsat)	30–60	1982–2009	Tornado dating	Free (but limit of 10 images per day); less expensive; daily imagery available	Lowest resolution; unlimited imagery with monthly fee

resolution of 10–60 m, was also used to detect historical tornado tracks for three separate years that preceded Planet imagery availability. In Google Earth, it was observed that historical tornado tracks became more difficult to detect approximately 11 years after occurrence because of satellite imagery resolution. The reason for this observation is not entirely known but may be due to forest regrowth, human development or logging, or a combination of these processes. Thus, it was determined that searches in Google Earth should be conducted for 1984 (earliest available Google Earth imagery), 1995 (+11 years), and 2006 (+11 years). An additional search in Google Earth in 2017 (+11 years) was not conducted because the higher resolution of Planet imagery would likely detect any tornadoes that occurred after 2006. Land Viewer was also used to date events. Land Viewer uses a myriad of different satellites including Landsat, Sentinel, MODIS, Pleiades, SPOT, Kompsat, and Superview. A summary of the satellite imagery used for tornado track detection and dating is given in Table 1.

Once a long, narrow region of tree damage was detected, or where there was an incident of large wind throws, it was noted and logged. These events were first cross-referenced with all known tornado events from NTP databases including the Tornadoes in Ontario Project (TOP) and Environment and Climate Change Canada's (ECCC's) National Severe Weather Database (NSWED). The TOP database is a draft database that contains tornado events that occurred within Ontario from the years 1792 to 2021. More information on this database can be found in Sills et al. (2022). NSWED contains tornado data for all provinces between 2003 and 2019.

TABLE 2. ECCC (post-2013) F-scale rating table.

EF scale	EF-scale wind speed (rounded to 5 km h^{-1})
0	90–130
1	135–175
2	180–220
3	225–265
4	270–310
5	315 or more

Once determined as new, events were assessed to determine if a tornado was the likely cause. This was done using the procedures documented in Sills et al. (2020): 1) major areas of forest damage are aligned, with no along-path gaps greater than 3 km (otherwise considered a new event); 2) aspect ratio of aligned damage path approaches 10:1 (length:width); 3) path width less than 2 km (with rare exceptions, however, no exceptions occurred in this study) and total length at least 1 km; and 4) can be a wider area of nontornadic damage in the vicinity, but mostly to one side of the tornado damage path. All cases that fit within all of these criteria were classified as tornadic, and those that did not were categorized as either a downburst or an "unclassified wind damage" event.

b. Estimating tornado intensity

Once an event was classified as tornadic, each event was viewed within Planet's 3.7-m daily imagery (events 2009 or later) to assess the tornadoes maximum width and length.

TABLE 3. DOD descriptions for expected (EXP), lower-bound (LB), and upper-bound (UB) maximum wind speed estimates (km h^{-1}) for the damage indicator of trees (C-2 Trees, or C-T). Additional notes (not shown) provide rating guidance.

DOD	Damage description	EXP	LB	UB
1	Small limbs broken (less than 2-cm diameter)	70	55	85
2	Large branches broken (2–8-cm diameter)	90	65	110
3	Up to 20% of mature trees snapped and/or uprooted	115	80	150
4	More than 20% of mature trees snapped and/or uprooted	150	105	190
5	More than 50% of mature trees snapped and/or uprooted	190	145	230
6	More than 80% of mature trees snapped and/or uprooted; numerous trees may be denuded/debarked by missiles with only stubs of largest branches remaining	235	190	275

TABLE 4. ECCC former (pre-2013) F-scale ratings (with speed range; km h^{-1}) and damage descriptions for shallow- and deep-rooted trees.

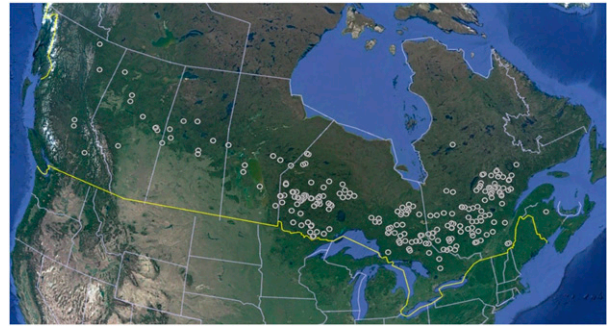| Code	Indicator	F0 (60–110)	F1 (120–170)	F2 (180–240)	F3 (250–320)	F4 (330–410)	F5 (420–510)	Notes
TS	Shallow-rooted trees	Large branches down; intermittent trees snapped at trunk or uprooted	Many trees snapped at trunk or uprooted	All trees along large path snapped at trunk or uprooted		Trees denuded and debarked by missiles		Assumes that trees are healthy and the ground is not sodden; root depth depends on species and subsurface types
TD	Deep-rooted trees	Large branches down	Intermittent trees snapped at trunk or uprooted	Many trees snapped at trunk or uprooted	All trees along large path snapped at trunk or uprooted	Trees denuded and debarked by missiles		Assumes that trees are healthy and the ground is not sodden; root depth depends on species and subsurface types

FIG. 2. Map of start locations of discovered historical tornadoes in Canada. The background image is provided by Google Earth.

Cloudless imagery was also selected to assess maximum path-length and maximum width, so the edges of the track were more easily seen. The 3.7-m resolution imagery allows for a more accurate estimate of width and length, although it is likely still a conservative estimate without higher-resolution imagery. If Planet imagery was not available, Google Earth or Land Viewer was used. When the date range of interest was earlier than 2009, Land Viewer imagery with resolutions between 30 and 60 m was most often used for analysis as the imagery could be zoomed very close to estimate the start and end points, and the maximum width. There is limited zoom within Google Earth historical imagery. Pathlength was defined as the length along the centerline of the damage and was calculated in Planet, Land Viewer, or Google Earth manually. The maximum width was also manually measured in Planet, Google Earth, or Land Viewer. The error associated with the pathlength and width measurements is in the tens of meters, because of satellite resolution. The weaker damage that likely occurred along the periphery of each event cannot be seen. Although debris cleanup can also impact the maximum path width and length measurements by making the measurements appear larger, cleanup was not a concern in this study region as most of the tornado events occurred in sparsely populated regions.
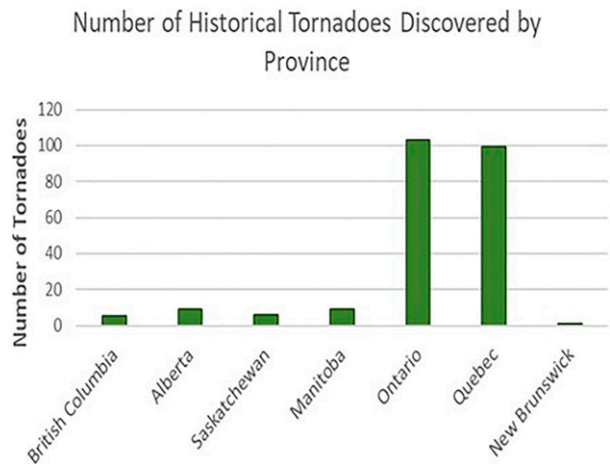

FIG. 3. Distribution of the number of historical tornadoes discovered by Canadian provinces.
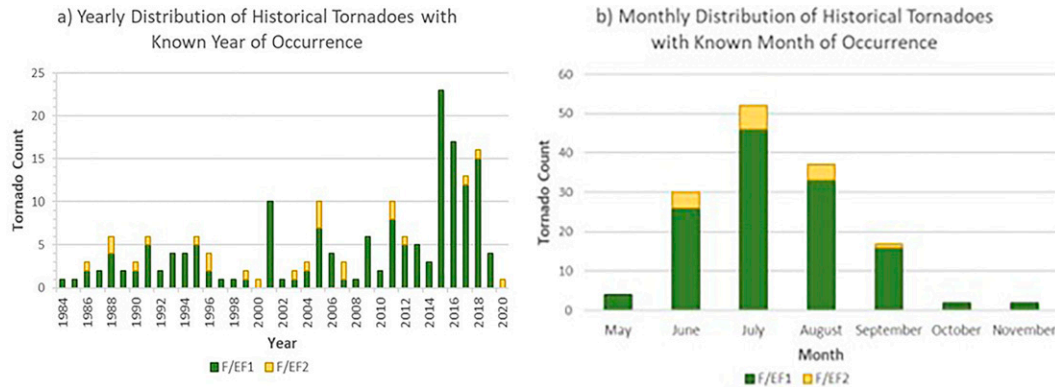
FIG. 4. (a) Yearly distribution of historical tornadoes for which an event year is known, and (b) monthly distribution of historical tornadoes with a minimum known month of occurrence.

For each tornado, the latitude and longitude of the start, worst damage, and end locations were obtained, as well as the direction of motion, the damage indicators, the degree of damage (events 2013 and later), the estimated wind speed (events 2013 and later), and the F/EF-scale rating. The method for estimating the F/EF-scale ratings is described in the following paragraphs.

The Fujita scale was developed by T. Fujita to estimate a tornado's wind speed using the damage left behind. This scale was used in Canada by ECCC up until 2012, when a modified version of the enhanced Fujita scale was developed for Canada and adopted starting in 2013. In general, the EF scale considers more damage indicators, such as different building types. For each damage indicator, there are degrees of damage that are used to estimate the maximum wind speeds and thus, EF-scale rating (Table 2). The modifications for the Canadian context included a refined damage indicator table for tree damage (Table 3). Any events that occurred prior to 2013 were rated using the former F-scale using ECCC's wind damage rating table for tree damage (Table 4) and are not assigned an estimated maximum wind speed.

EF-scale ratings were determined using NTP's forest box method [refer to Sills et al. (2020)]. The forest box method involves creating a contour around the detected damage track and identifying its centerline. Once the maximum path width is determined, a sampling box is created that is 50% of the maximum path width distance on all sides. This box is then placed at various locations along the centerline to find the area of worst damage to estimate the percentage of trees uprooted and/or snapped and determine the degree of damage (DOD) from the damage indicator table for trees. The estimated wind speed is determined using Tables 3 or 4 (depending on the year of occurrence), which is then used to determine the F/EF-scale rating and maximum wind speed (Table 2), if applicable. Ratings are typically restricted to F/EF1 and F/EF2. F/EF0 damage is rarely seen with satellite imagery at the given resolution and F/EF3 damage is difficult to achieve in forests on the Canadian Shield due to mostly shallow soils. Within the Canadian Shield (which extends

from Labrador and continues west to a portion of northern Alberta; Barrett 2022), underneath the boreal forest is granite rock. As a result, tree roots are shallow and grow laterally. Strong and La Roie (1983) conducted a study showing that in the boreal forests of Alberta, lateral root growth (shallow), also dominated the root system of all species of trees within the region. As a result, it was assumed that all trees within the study area were shallow rooted.

c. Determining tornado event date

Events were dated using a combination of satellite imagery (Planet, Land Viewer, and Google Earth), historical radar (where available), and lightning data (used minimally), along with archived U.S. Storm Prediction Center (SPC) mesoanalysis products. However, in the regions where tornadoes were detected, the earliest satellite imagery available is 1982. As such, although some of the discovered events were years old and could be detected in the 1982 satellite imagery, they could not be traced back to a date of occurrence and, as a result, have not been assigned a date. Some events have also been dated by just a year or a month within a year. A date range was initially determined for each tornadic event using the available satellite imagery. Planet has imagery available back to 2009; for events prior to 2009, Land Viewer was used to help date events. Google Earth was only helpful to narrow to
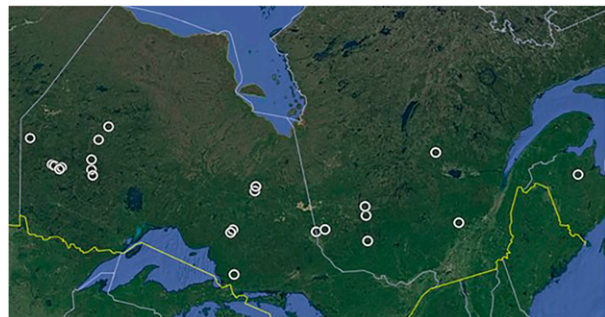

FIG. 5. Map of all 2015 historical tornado events. The background image is provided by Google Earth.
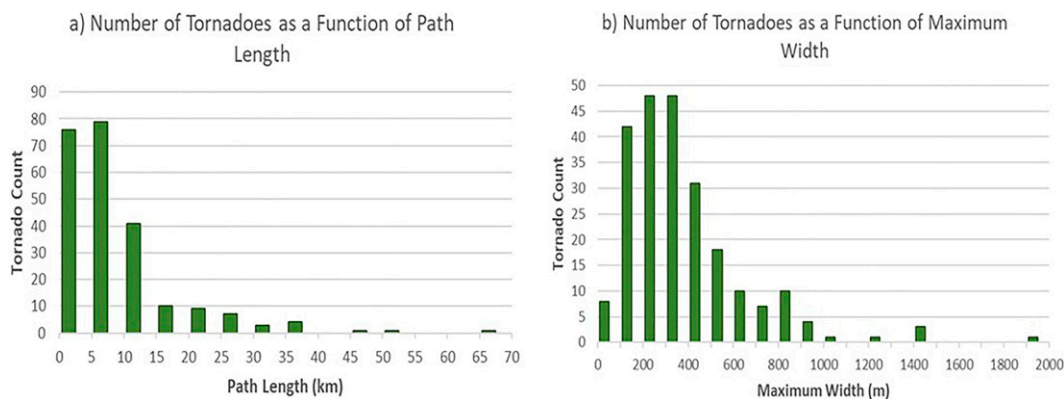
FIG. 6. Number of tornadoes as a function of (a) pathlength and (b) maximum width.

a specific year during the initial tornado searches. However, Google Earth may not show tornado tracks in the year that they occurred because of the time of year when satellites take the imagery. Later-season tornadoes are often not seen until the following year. Unfortunately, dating of tornado events was often hindered by imagery availability and cloud cover. Cloud cover was an issue for most events, but clear imagery eventually appeared for all events. However, for several events, this made dating events within a short window difficult if cloud cover was combined with limited image availability. There were several events that included date ranges from 3 to 10 months. However, most cool- and cold-season months could be ruled out because conditions are generally not favorable for tornado development, and thus they were excluded when dating the historical events.

For events for which dates could be narrowed down, meteorological conditions associated with potential tornado formation were analyzed using archived SPC mesoanalysis products. The common products used were the Supercell Composite Parameter (SCP) and Significant Tornado Parameter (STP) (used less often). In short, SCP and STP composites are meant to highlight regions where ingredients favor supercell development and supercells capable of producing F2-F5 tornadoes, respectively (Thompson et al. 2004). Based on the results of Thompson et al. (2003, 2007, 2012), Gallus et al. (2008), Grams et al. (2012), and Trapp et al. (2005), the environmental differences between supercell and linear convective modes are small. Thus, SCP is not able to discriminate between these two storm modes in which tornadoes most often occur. As such, this was the main mesoanalysis product used to identify tornado days. However, archived SPC data are only available as far back as 2005, so this tool helped only to narrow dates from 2005 onward.

Once possible event dates were narrowed, historical radar data provided by ECCC was used to find severe storms that were the likely culprit for the forest disturbance. This was done by overlaying the radar image in Google Earth over the location of the noted track. ECCC radars are C band (except McGill, Quebec, Canada, which is S band) (although some have already been upgraded to S band); they have a range of 240 km, a spatial resolution of 1 km, and a temporal resolution of 10 (C band) and 6 (S band) min. However, the

upgrading to S band occurred outside the scope of this paper, so C-band radar imagery is the radar tool used for date assessment. Using this tool, a specific date and time could be assigned to events. ECCC radar imagery is only available from 2007 onward; thus, all events could be dated between 2007 and 2020. However, dating became difficult prior to 2007. For events between 2005 and 2007, synoptic-scale setups were analyzed using SPC mesoanalysis products (surface maps and SCP) to fully date events. Prior to 2005, events have been dated by either a month or a year or were not dated because of limited data. Because of a lack of data, there is a greater uncertainty in the date of occurrence the farther back in time we go. The use of U.S. WRS-88D data was not investigated because many of the tornado events occurred in the northern portions of Canada, nowhere near the U.S. border. Of those events that did occur near the U.S. border, there was enough radar coverage with ECCC data to date events.

Lightning data were used very minimally for events that fell outside radar range but also occurred in the year 2016 or later.
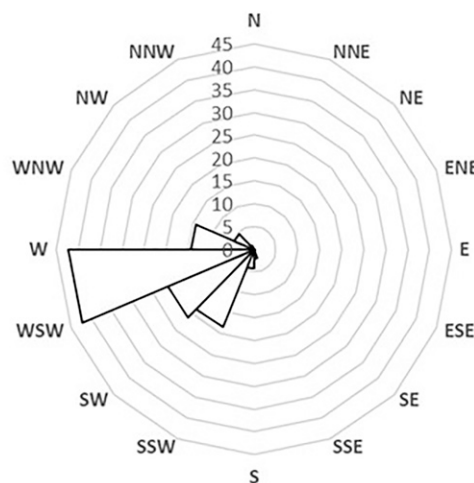

FIG. 7. Direction of motion from which the 231 identified Canadian historical tornadoes originated. Circle contours denote percentage of events.

TABLE 5. The top 10 tornadoes with the largest pathlength as estimated by satellite imagery. The start and end points are in degrees of latitude and longitude.

Event name	Date (UTC)	Start point	End point	Pathlength (km)	Max width (m)	F-scale rating
Wrist Lake	Pre-1982	50.7871, −94.8191	51.0899, −94.0210	65.9	1930	2
Carnarvon	Pre-1982	45.0508, −78.7930	45.1626, −78.1421	53.0	600	2
Hood Lake	24 Jun 2005	50.7817, −89.7931	50.9740, −89.2330	47.0	1440	2
Murdoch Lake	Pre-1982	48.3478, −91.3908	48.3790, −90.8752	39.7	1230	2
Frog Lake	1991	48.2624, −83.0134	48.2655, −82.5490	35.3	870	2
Lac Cullin	Pre-1982	46.3540, −77.8337	46.2957, −77.4252	32.2	1090	2
Lower Aitken Lake	1988	48.8107, −82.1064	48.7468, −81.7303	28.8	960	2
Perrigo Lake	Pre-1982	50.9517, −92.8284	51.1191, −92.4980	26.7	1430	2
Thurman Lake	August 1996	51.1933, −88.2489	51.2331, −87.8103	26.1	1480	2
Lac Manouane	Pre-1982	50.1519, −71.1892	50.1214, −70.8354	25.8	810	2

The lightning data were acquired through LightningMaps.org. This website is generated by Blitzortung.org, which is a lightning detection network consisting of more than 500 lightning receivers that measure electromagnetic discharges in the atmosphere with very low frequency (VLF) receivers based on the time of arrival and time of group arrival method. See Vahabi-Mashak et al. (2015) and Dowden et al. (2002) for more information on the methods.

3. Results

a. Distribution of historical tornadoes

After the comprehensive search across Canada, 231 previously unknown tornadoes were identified (Fig. 2). The majority of these tornadoes were found in the heavily forested regions of Ontario and Quebec. In Alberta, Saskatchewan,

and Manitoba, most events were found in the northern sections of Alberta, Saskatchewan, and Manitoba. There are a few exceptions that were found farther south; however, these events were still discovered in areas with a large percentage of trees. A small number of historical events were found in British Columbia and New Brunswick. No tornadic events were discovered in the Yukon, Northwest Territories, Nunavut, Prince Edward Island, Nova Scotia, or Newfoundland and Labrador.

The majority of the identified historical tornado tracks (201 of 231) are found in Ontario and Quebec. This is likely due to these regions being more heavily forested than Alberta, Saskatchewan, and Manitoba. As noted earlier, tornado damage of F/EF1 or greater intensity is likely more evident in forested regions than in terrain such as grassland or low-forested areas (Shikhov and Chernokulsky 2018) as a result of the current resolution of satellite imagery. In addition, the Pacific (British Columbia) and Atlantic provinces (New Brunswick, Nova Scotia, Prince Edward Island, and Newfoundland and
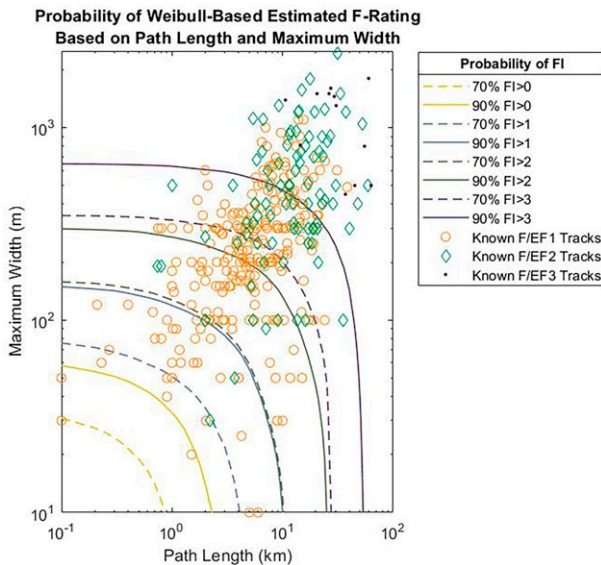

FIG. 8. Estimated probabilities of exceedance for different F-scale intensities based on Brooks (2004), Shikhov and Chernokulsky (2018), and Rodríguez and Bech (2020). Solid lines represent 90% probability, and dashed lines represent 70% probability. Known Canadian F/EF1, F/EF2, and F/EF3 tornadoes (1991–2020) are overlaid.
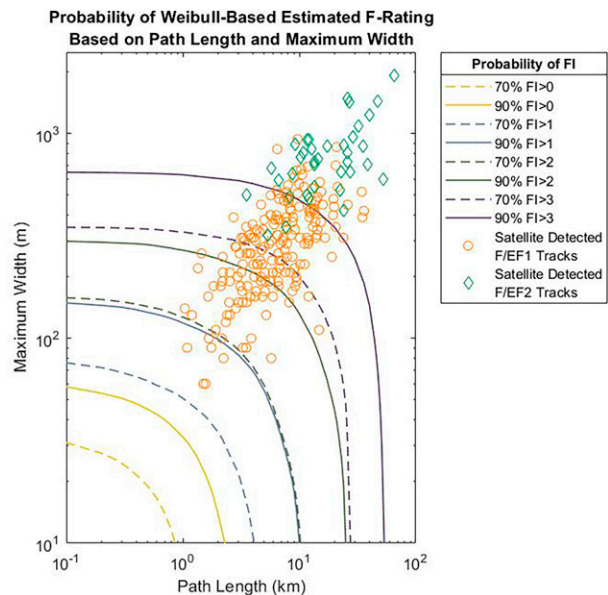

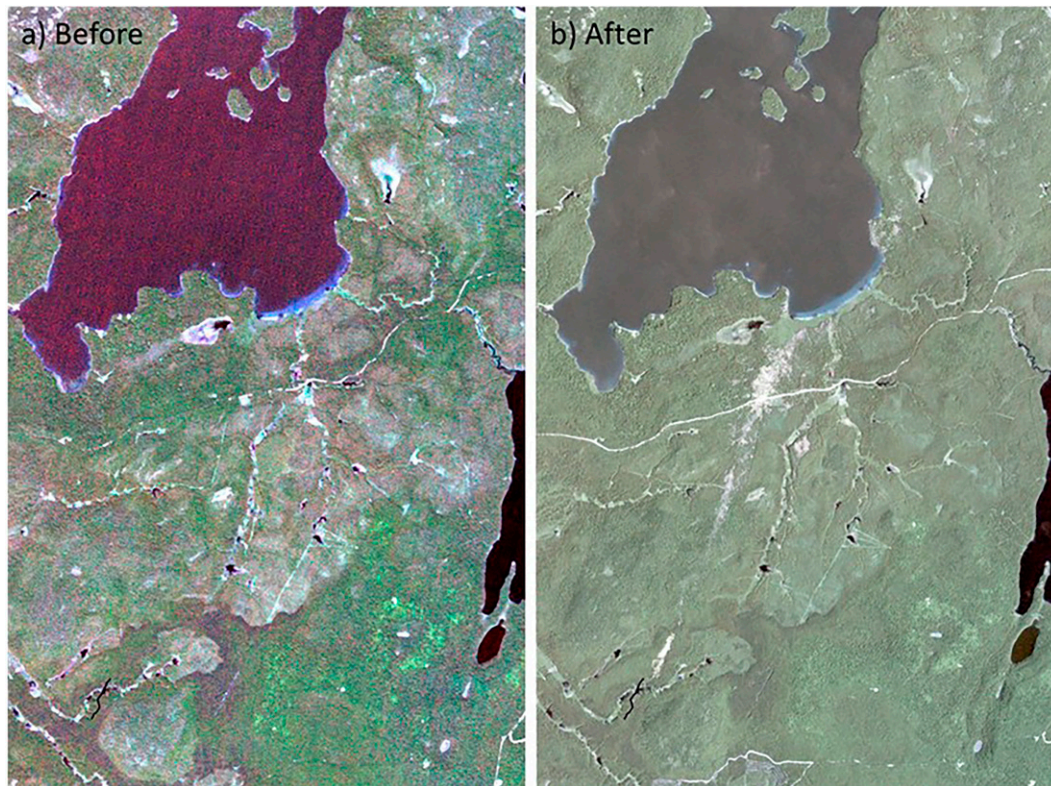FIG. 9. As in Fig. 8, but with discovered Canadian historical F/EF1 and F/EF2 tornadoes overlaid.

FIG. 10. (a) "Before" and (b) "after" high-resolution Planet satellite imagery of the Lac Caire tornado. Imagery was collected for (a) 13 Aug 2015 and (b) 29 Jun 2016; 29 Jun 2016 was the first available date of unobscured (cloudless) imagery of the entire tornado track during a warmer month.

Labrador) are typically not favorable environments of tornado formation. British Columbia, which has an average tornado rate of 0.6 per year (using 1980–2009 data), often has a high pressure system over the Pacific Ocean during the summer months that does not allow for strong extremes of temperature and moisture needed to fuel tornadoes. The Atlantic provinces have an average of just 1.2 tornadoes per year. This is due to these areas having such small landmasses while also being surrounded by the Atlantic Ocean. As a result, the necessary heating over land to fuel storms does not occur as often, coupled with the surrounding ocean waters remaining cool. Without the extreme heating needed to fuel tornado-producing storms, tornadoes are a relatively rare occurrence in the Atlantic provinces. However, although tornado occurrence is unfavorable in these regions, all of the boxes that covered the Atlantic provinces and British Columbia were searched that contained large enough tree cover (more than 25%).

b. Historical tornado climatology

A breakdown of newly discovered historical tornadoes by province is as follows: 103 for Ontario, 98 for Quebec, 9 for Manitoba, 6 for Saskatchewan, 9 for Alberta, 5 for British Columbia, and 1 for New Brunswick (Fig. 3). The number of tornadoes discovered between 2017 and 2020 does not include events that were found separately by NTP. The count would be larger if NTP had not formed. The largest number of

discovered tornadoes occurred in 2015 (Fig. 4a), and the largest number of F2 tornadoes occurred in 2005. Of all historical events found, the months of occurrence spanned from May through November (Fig. 4b). The earliest event occurred on 4 May 2018 (rated EF1), and the latest event, which was a two-tornado event, occurred on 6 November 2015 (both rated EF1). The maximum tornado frequency is observed in July for both F/EF1 and F/EF2 ratings. This result supports the climatological studies of Cheng et al. (2015) and ECCC (2020). Stronger tornado events (F/EF2) stretched from June through September.

Although 2015 did not begin as a stormy year in the eastern portion of the country, storms began to increase in August with the development of a heat wave (Canadian Meteorological and Oceanographic Society 2015). This shift in weather coincides with the dating of the Ontario, Quebec, and New Brunswick events in 2015, where 18 of the 23 events discovered for that year occurred between August and November (Fig. 5).

More than 50% of discovered tornadoes, 155 of 231, have a pathlength of less than 10 km (Fig. 6a), which is expected for events rated F/EF1 and F/EF2, according to ECCC (2020), Groenemeijer and Kuhne (2014), Shikhov and Chernokulsky (2018), and Malamud and Turcotte (2012). Based on pathlength analysis, there were 10 tornadoes with a track greater than 30 km, with the largest being 65.9 km. This event has not been dated because it occurred prior
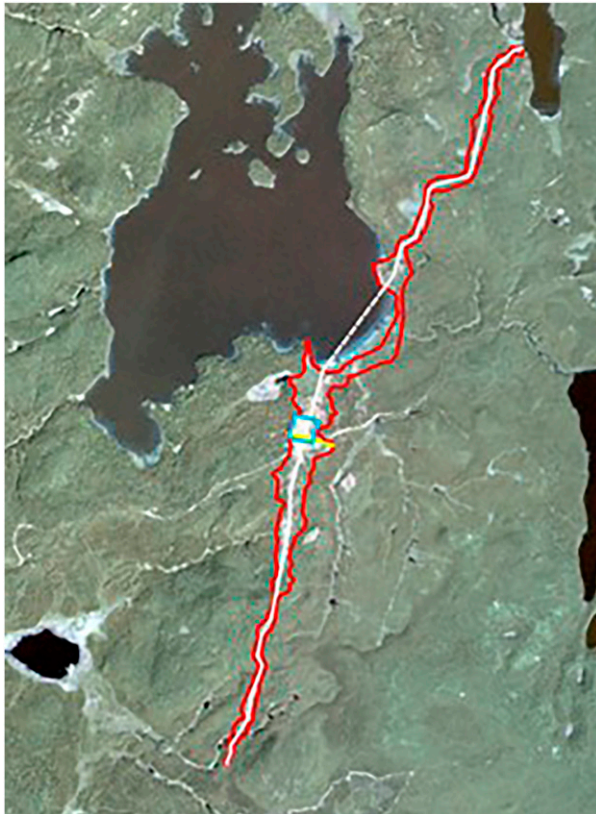
FIG. 11. Path outline (red), centerline (white), and maximum width (yellow) of the Lac Caire tornado. The image was collected from Planet for 29 Jun 2016. The path outline was added in the ArcGIS software.

to 1982, but it was given an F2 rating. The shortest track length is 1.1 km for a tornado that occurred in Saskatchewan in 2003.

Most tornado tracks have widths between 200 and 300 m (48) and 300 and 400 m (48), followed by 100 and 200 km (42) (Fig. 6b). According to ECCC and U.S. data, these path widths are typical for F1 and F2 tornadoes (ECCC 2020; Groenemeijer and Kuhne 2014; Shikhov and Chernokulsky 2018). However, there were 6 tornadoes with a path width greater than 1000 m, which were all associated with stronger F2 tornadoes. Four of these events occurred prior to 1982, while one occurred in August 1996 and the other on 24 June 2005.

Overall, the direction of motion from these tornadoes is primarily from the west [consistent with analysis conducted by ECCC (2020)], followed by the west-southwest and south-west, respectively (Fig. 7). This prevailing direction is consistent with additional analysis conducted by Newark (1988) who found a westerly prevailing wind direction in Ontario and Quebec, while in Alberta, Saskatchewan, and Manitoba it is from the southwest.

In comparing ECCC's NSWED (2003–19) with the historical search results of the same time period, it is seen that the percentage increase in tornado counts in Canada's provinces are +2.98% for Alberta, +200% for British Columbia, +3.64% for Manitoba, +6.25% for New Brunswick, +15.82% for Ontario, +45.35% for Quebec, and +1.82% for Saskatchewan. These results exclude all historical tornadoes that were detected prior to 2003 and after 2019. The NSWED data only cover 2003–19, so historical tornadoes that occurred outside this date range were excluded to compare how many tornado events were missed during the same time. These additions represent a substantial increase to tornado counts, especially in Ontario, Quebec, and British Columbia, and the majority of these events occurred in regions with sparse populations. It is unsurprising that the percentage increases are lower in Alberta, Saskatchewan, and Manitoba, as historical tornadoes are much more difficult to detect because of a lack of large forested regions. The 6.25% increase in New Brunswick is the result of adding one new event to the database.

c. Event dates

Using the dating method described in section 2, 125 events were successfully dated, 19 were dated by only a month, 41 were dated by only a year, and 46 remained undated because they occurred prior to the earliest available satellite imagery used for detection. The tornadoes with the 10 longest pathlengths are summarized in Table 5.

FIG. 12. (a) Square box in ArcGIS with side lengths of 280 m placed along the centerline of the Lac Caire tornado over the area of worst damage. (b) Zoomed-in view of the box, with the shaded areas representing areas without any noticeable tree damage.
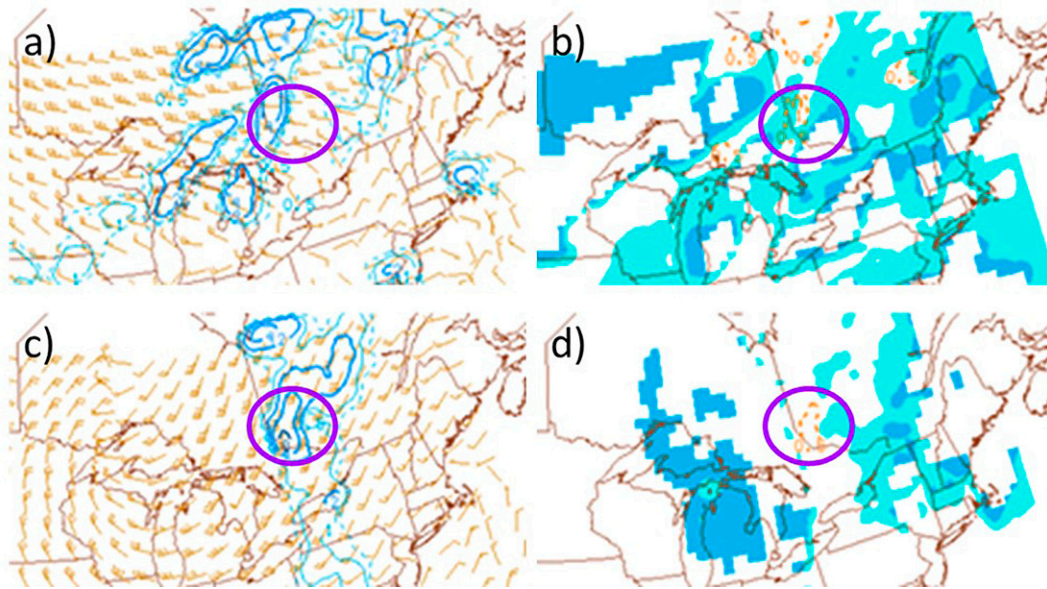
FIG. 13. (left) SCP and (right) the STP for (a),(b) 17 and (c),(d) 20 Aug. The tornado occurrence is within the purple circle. Mixed-layer CIN (MLCIN) is shaded in (b) and (d).

d. Evaluation of tornado intensity using an alternate method

Another way to estimate tornado intensity as shown by Shikhov and Chernokulsky (2018) is to relate it to tornado path characteristics (Pisnichenko 1994). Brooks (2004) applied a Weibell distribution to model tornado pathlengths and widths for different F-scale ratings using SPC data from more than 40 000 cases. It can be considered as appropriate to apply U.S. statistics to Canadian regions because of their close proximity and northern extension of similar tornadic storm environmental conditions.

To calculate the probability of a tornado's F rating given a pathlength or width, the distributions calculated using the Weibull probability distribution function as described in Brooks (2004) are weighted by the number of tornadoes at each F scale (given in Brooks 2004). They are then divided by the sum of the weighted distributions for pathlength or width (Brooks 2004). According to Brooks (2004) (using only SPC data), for events with a pathlength of 30 km, 1% of them are rated F0, 26% are rated F1, 43% are rated F2, and 23% are rated F3. As noted by Brooks (2004), F5 tornadoes are never the most likely rated event because of their rarity of occurrence. On the other hand, for events with widths exceeding 1000 m, the most rated events are F2 (25%), F3 (25%) and F4 (45%). Once again, because of the rareness of F5 events, only 5% of events with a 1000-m width are given this rating. The results of Brooks (2004) continue to be consistent with
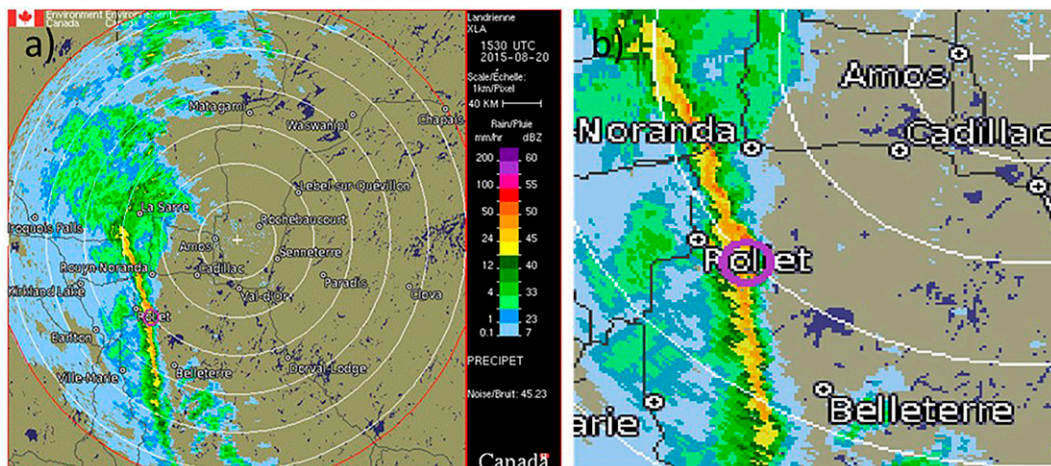

FIG. 14. ECCC (a) historical radar [Landrienne (XLA)] for 1530 UTC 20 Aug 2015. The purple circle indicates the approximate Lac Caire tornado start location. (b) A zoomed-in view of (a).
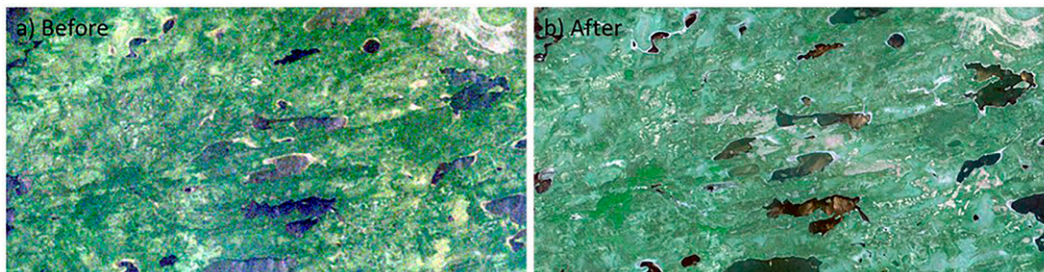
FIG. 15. The (a) before and (b) after high-resolution Planet satellite imagery of the Orell Lake tornado. Imagery was collected for (a) 14 Jul 2004 and (b) 12 Jun 2011.

the latest literature, in which stronger tornadic events have wider widths (Marion 2017; Trapp et al. 2017; Shikhov and Chernokulsky 2018; Wurman et al. 2021).

Brooks (2004) had noted that an exact F-scale rating could not be determined using the data, therefore, Shikhov and Chernokulsky (2018) as well as Rodríguez and Bech (2020) used the probability of exceedance to determine the probability of a minimum tornado F-scale rating for each pathlength and maximum width. The results of the probability of exceedance method and NTP's forest box method were compared to ascertain consistency and reliability of the results, as shown in Figs. 8 and 9. Figure 8 shows the probability of exceedance curves, which were produced by Rodríguez and Bech (2020), overlaid with Canadian tornado data (1991–2020) for tornadoes with both a known track length and maximum path width with F/EF-scale ratings ranging from F/EF1 to F/EF3. Similar to Fig. 8, Fig. 9 shows the track length and maximum path width data for the newly discovered historical tornadoes with F/EF-scale ratings of F/EF1 and F/EF2.

As seen in Figs. 8 and 9, the rating of historical events appears to be consistent with ratings conducted across Canada from 1991 to 2020. This result was expected. However, there does appear to be an underrating of events based on the data, however, this underrating is likely a result of the primary damage indicator being trees for all newly discovered historical events. Based on the damage indicator rating table and known Canadian terrain characteristics, such as shallow-rooted trees in Canada's boreal forests (552 million hectares of forest that stretches from the east coast of Newfoundland to the west coast of Yukon; Natural Resources Canada 2020), the largest an event can be rated based on the damage indicator of trees in the study area is EF2. A new EF-scale standard is being developed under the auspices of the American Society of Civil Engineers (ASCE), with the help of NTP, that will have more sophisticated methods for assessing tree damage. It is important to note that Figs. 8 and 9 represent a probability of a minimum tornado intensity and therefore cannot be used as a replacement for high-quality damage surveys that determine the actual tornado intensity.

e. Methodology case studies: Lac Caire, Quebec, and Orell Lake, Ontario

To demonstrate the identification process, NTP's forest box method, and the dating methodology used, two case studies

are described in more detail: Lac Caire, Quebec, and Orell Lake, Ontario.

1) LAC CAIRE (20 AUGUST 2015)

A previously unknown long and narrow region of tree damage was detected in western Quebec. "Before" and "after" high-resolution satellite images of the damage are shown in Fig. 10. Using the methodology described in section 2, the tornado path outline, centerline, and maximum width of the track are plotted (Fig. 11). For this event, the pathlength was estimated at 7.99 km with a maximum path width of 560 m. This meets the necessary criteria needed to be considered a tornado event as described in Sills et al. (2022). Using NTP's forest box method, a box with a size that is 50% the maximum width (280 m), was placed along the centerline of the track to find the area with the worst damage (Fig. 12).

Using ECCC's damage indicator table (Table 3), approximately 55% of trees are damaged (Fig. 12b). Using a lower bound of wind damage due to the soil characteristics of the Canadian Shield, the estimated maximum wind speed is 145 km h^{-1} (Table 3), which equates to an EF1 tornado.

Planet satellite imagery was used to narrow the date of occurrence to between 13 and 22 August 2015. Once the date range was determined, archived SPC mesoanalysis tools, the SCP and STP, were used to further refine the potential storm date to either 17 August or 20 August (Fig. 13). SCP was the primary product used for this event, but the STP was used as an additional aid since there were several possible dates
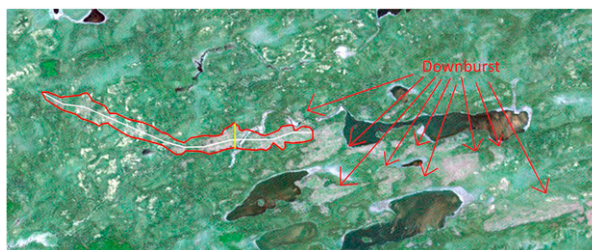

FIG. 16. Path outline (red), centerline (white), and maximum width (yellow) of the Orell Lake tornado. Additional downburst damage is noted with red arrows. The image was collected from Planet for 12 Jun 2011. The path outline was added in ArcGIS.
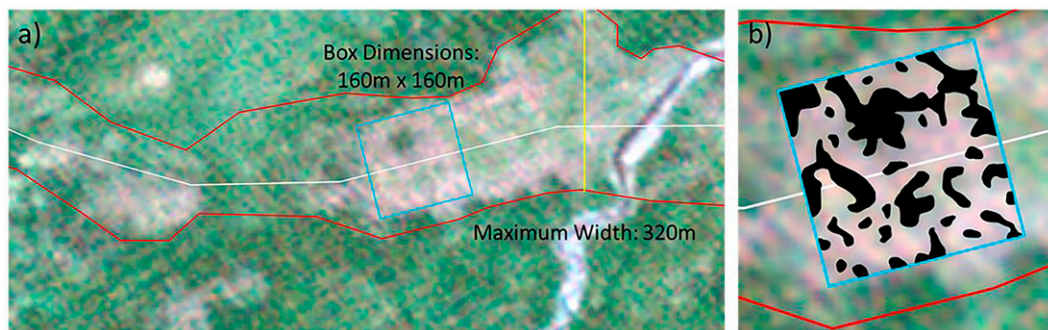
FIG. 17. (a) Square box in ArcGIS with side lengths of 160 m placed along the centerline of the Orell Lake tornado over the area of worst damage. (b) Zoomed-in view of the box, with the shaded areas representing areas without any noticeable tree damage.

of tornado occurrence. The STP helped to narrow the likely event date down to 17 or the 20 August. ECCC historical radar imagery was then utilized to search for storms that tracked over the area of interest. Once a storm candidate was detected (20 August), it was overlaid in Google Earth over the noted start location of the tornado track. Using this overlay process, the start time of the event was estimated at 1520 UTC (Figs. 14a,b). Although storms did develop on 17 August, they did not occur over the location of the tornado.

2) ORELL LAKE (5 SEPTEMBER 2005)

A long and narrow region of tree damage was detected in northwestern Ontario. Before and after imagery are seen in Fig. 15. Using the methodology described in section 2, the tornado path outline, centerline, and maximum width of the track are plotted (Fig. 16). For this event, the path-length was estimated at 3.72 km with a maximum path width of 320 m. Although this event was more of a challenge to assess because the event appeared to make a transition to a downburst, it still met the criteria needed to be considered as a tornado event as described in Sills et al. (2020).

Using NTP's forest box method, a square box with a size that is 50% the maximum width (160 m), was placed along the centerline of the track to find the area with the worst damage (Fig. 17). However, since this event occurred in 2005, prior to the introduction of the EF scale, the former F scale (Table 4) must be used to estimate the tornado intensity. Using the table, this event was rated F1 because 100% of trees were not uprooted but more than 60% of trees were damaged.

Land Viewer satellite imagery was used to narrow the date of occurrence to between 18 August and 27 September 2005. The archived SPC mesoanalysis tools SCP and STP were used to further refine the potential storm dates to 5, 11, 20, and 26 September (Fig. 18).

Historical ECCC radar was unavailable in 2005; thus the STP tool, which looks for environments more favorable for tornado development, was used to further narrow the four

noted dates to 5, 11, or 20 September (Figs. 18b,d,f). Archived SPC visible satellite imagery was used to detect whether storms developed over the region on these dates. Storms began to form around 2115 UTC 5 September (Fig. 19a), weaker single-cell storms appeared on 20 September (Fig. 19c), and no storms appeared to extend far enough north over the region on 11 September (Fig. 19b). However, these data are limited to the visible spectrum, so nocturnal storms would not be detected. Assessing nearby weather station data, Pickle Lake A, which is the closest station with available data, 5 September contained reports of thunderstorms (ECCC 2022a), 20 September contained reports of "mostly cloudy" (ECCC 2022c), and 11 September contained reports of "mainly clear" (ECCC 2022b). Thus, 5 September was chosen as the likely date of occurrence. However, a time could not be confidently assigned because of minimal data.

f. Dating methodology accuracy check

To determine the accuracy of the dating methodology employed throughout the paper, three tornadoes within the known Ontario tornado dataset (from TOP) were randomly chosen and the above dating methodology was applied. The three tornadoes selected were named Ear Falls, Goose Lake, and Sioux Lookout, and the results of the accuracy check are summarized in Table 6. For both Ear Falls and Sioux Lookout, the use of satellite imagery, archived SPC mesoanalysis SCP product, and historical ECCC radar were utilized. With Goose Lake, only satellite imagery could be applied to determine a date range because of the year of occurrence. However, based on the results of the three randomly chosen known tornadoes, the dating methodology appears to be fairly accurate in determining the likely date of tornado occurrence.

4. Limitations

Canada is a large region to manually scan; however, the country was scanned using Planet's monthly mosaicked August imagery in 2019 and 2020. Using Google Earth imagery, it appeared that many tornado tracks became undetectable around the 11-yr age mark. The reason for this observation is unknown but may be due to regrowth, land-use
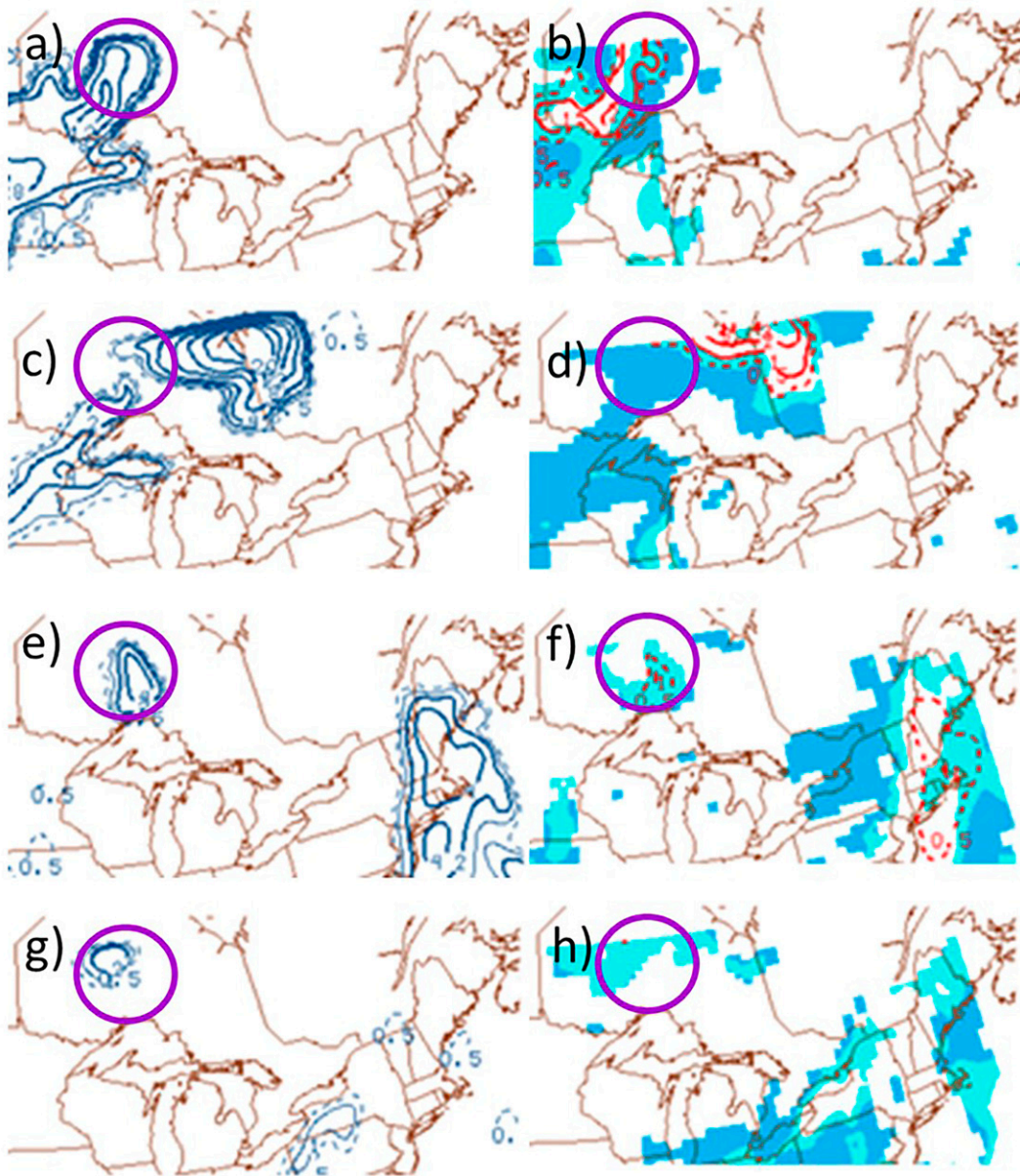
FIG. 18. (left) SCP and (right) the STP contours for (a),(b) 5, (c),(d) 11, (e),(f) 20, and (g),(h) 26 Sep. The tornado occurrence is within the purple circle. MLCIN is shaded in (b), (d), (f), and (h).

change, and/or logging. Therefore, additional scanning was completed using Google Earth in 1984, 1995, and 2006, which was a very time-consuming endeavor. It may be possible that tornado events were missed that occurred between these search years.

Dating historical events is difficult for events that occurred prior to 2005. Minimal data are available, but the use of historical weather maps is being investigated to date some of these older events in which no additional data are available other than a month or a year. Currently, it appears unlikely that a date can be given to events that occurred prior to the available 1982 satellite imagery.

Using satellite imagery limits the scope of tornadoes discovered. Current satellite imagery is too coarse to detect weaker events, such as EF0. There are likely numerous events that were not discovered through searching satellite imagery. This issue may get resolved as imagery resolution improves.

5. Conclusions

A large-scale, systematic search of Canada's forested regions was conducted using high-resolution satellite imagery resulting in 231 previously unknown historical tornadoes being discovered. Satellite imagery was also used to estimate
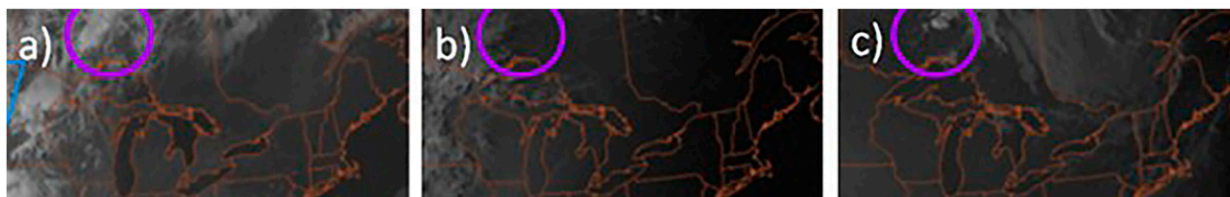
FIG. 19. Archived SPC visible satellite imagery for (a) 2125 UTC 5 Sep 2005, (b) 2315 UTC 11 Sep 2005, and (c) 2225 UTC 20 Sep 2005. The area of the tornado occurrence is circled in purple.

tornado pathlength, maximum path width, estimated wind speed, F/EF-scale rating, and the direction of motion. When possible, events were dated using archived SPC mesoanalysis data, lightning data, historical ECCC radar imagery, and surface maps. This method resulted in 125 events being successfully dated, whereas 19 were dated only by month and 41 only by year; 46 remained undated because they occurred prior to available satellite imagery. Of all events, 103 occurred in Ontario, 98 in Quebec, 9 in Manitoba, 6 in Saskatchewan, 9 in Alberta, 5 in British Columbia, and 1 in New Brunswick.

A method for estimating tornado intensity using pathlength and width values and Weibull distributions (based on U.S. data) was used to evaluate the intensity estimation method used for this study (NTP's forest box method). Results indicate a relatively consistent evaluation of events, providing reassurance of the rating method used by NTP.

According to the analysis, July is the most common month for tornadoes for both lower end (F/EF1) and higher end (F/EF2) tornadoes. The results are consistent with Cheng et al. (2015), who noted that the peak tornado season in Canada occurs in July, with hotspots in Alberta, Saskatchewan, Manitoba, and Ontario. Also consistent with previous research is the direction of motion of tornadoes, with the predominant direction from the west (more than 45% of all events). When broken down by region, in Ontario and Quebec this percentage adjusts to 34% and in Alberta, Saskatchewan, and Manitoba it adjusts to 29%. The second largest direction of motion in Alberta, Saskatchewan, and Manitoba is from the southwest (17%), which is consistent with previous literature.

The largest number of historical tornadoes was discovered in 2015 (22), however, all events were rated EF1. The largest number of stronger events was discovered in 2005 (4). More than one-half of all historical tornadoes have pathlengths less

than 10 km, and maximum path widths are between 100 and 400 m, which is also consistent with U.S. observations. Of note, it is possible that the stronger F/EF2 tornadoes may have had a higher rating had they not occurred in a forest on the Canadian Shield.

These data will improve Canada's tornado climatology, although it is only a small subset and does not include weaker tornadic events that could not be identified with current satellite imagery. In addition, numerous downbursts events were detected while searching for the historical tornadoes. These events are being assessed and will be included in a future downburst database.

Data availability statement. The NTP tornado data used here are available via a public data portal at the link provided (https://doi.org/10.5683/SP3/53WFLM). Please contact Environment and Climate Change Canada with regard to NSWED data.

TABLE 6. Summary of the accuracy check of the methodology used to date historical tornadoes throughout the paper. Randomly selected tornadoes from the known Ontario tornado database (from TOP) include Ear Falls, Goose Lake, and Sioux Lookout.

	Results of dating methodology	Actual date of occurrence from TOP
Ear Falls	0130 UTC 10 Jul 2009	0135 UTC 10 Jul 2009
Goose Lake	Between 24 Jun 2003 and 17 Jul 2003	1800 UTC 4 Jul 2003
Sioux Lookout	2100 UTC 16 Aug 2011	2123 UTC 16 Aug 2011

REFERENCES

Barrett, D., 2022: Canadian Shield. The Canadian Encyclopedia, accessed 25 August 2022, https://www.thecanadianencyclopedia.ca/en/article/shield.

Bech, J., M. Gayà, M. Aran, F. Figuerola, J. Amaro, and J. Arús, 2009: Tornado damage analysis of a forest area using site survey observations, radar data and a simple analytical vortex model. *Atmos. Res.*, **93**, 118–130, https://doi.org/10.1016/j.atmosres.2008.10.016.

Brooks, H. E., 2004: On the relationship of tornado pathlength and width to intensity. *Wea. Forecasting*, **19**, 310–319, https://doi.org/10.1175/1520-0434(2004)019<0310:OTROTP>2.0.CO;2.

Burow, D., H. V. Herrero, and K. N. Ellis, 2020: Damage analysis of three long-track tornadoes using high-resolution satellite imagery. *Atmosphere*, **11**, 613, https://doi.org/10.3390/atmos11060613.

Canadian Meteorological and Oceanographic Society, 2015: Canada's top ten weather stories for 2015. CMOS Doc., 25 pp., https://cmos.in1touch.org/uploaded/web/website/top_ten/EN_Final%20Top%20Ten%20Weather%20Stories%20in%202015.pdf.

Cheng, V. Y. S., G. B. Arhonditsis, D. M. L. Sills, H. Auld, M. W. Shephard, W. A. Gough, and J. Klaassen, 2013: Probability of tornado occurrence across Canada. *J. Climate*, **26**, 9415–9428, https://doi.org/10.1175/JCLI-D-13-00093.1.

——, ——, D. Sills, W. Gough, and H. Auld, 2015: A Bayesian modelling framework for tornado occurrences in North America. *Nat. Commun.*, **6**, 6599, https://doi.org/10.1038/ncomms7599.

Chernokulsky, A., and A. Shikhov, 2018: 1984 Ivanovo tornado outbreak: Determination of actual tornado tracks with satellite data. *Atmos. Res.*, **207**, 111–121, https://doi.org/10.1016/j.atmosres.2018.02.011.

——, and Coauthors, 2021: Tornadoes in Russian regions. *Russ. Meteor. Hydrol.*, **46**, 69–82, https://doi.org/10.3103/S10683739 21020023.

Dowden, R. L., J. B. Brundell, and C. J. Rodger, 2002: VLF lightning location by time of group arrival (TOGA) at multiple sites. *J. Atmos. Sol.-Terr. Phys.*, **64**, 817–830, https://doi.org/10.1016/S1364-6826(02)00085-8.

Dyer, R. C., 1988: Remote sensing identification of tornado tracks in Argentina, Brazil, and Paraguay. *Photogramm. Eng. Remote Sens.*, **54**, 1429–1435.

ECCC, 2020: Canadian Tornado fact sheet. Government of Canada, accessed 15 January 2020, https://data-donnees.ec.gc.ca/data/weather/products/canadian-national-tornado-database-verified-events-1980-2009-public/CanadianTornadoFactSheet.pdf.

——, 2022a: Hourly data report for September 05, 2005: Pickle Lake A. Government of Canada, accessed 2 March 2022, https://climate.weather.gc.ca/climate_data/hourly_data_e.html?StationID=10251&timeframe=1&StartYear=1840&EndYear=2019&type=line&MeasTypeID=meantemp&wbdisable=true&time=LST&time=LST&Year=2005&Month=9&Day=5#.

——, 2022b: Hourly data report for September 11, 2005: Pickle Lake A. Government of Canada, accessed 2 March 2022, https://climate.weather.gc.ca/climate_data/hourly_data_e.html?StationID=10251&timeframe=1&StartYear=1840&EndYear=2019&type=line&MeasTypeID=meantemp&wbdisable=true&time=LST&time=LST&Year=2005&Month=9&Day=11#.

——, 2022c: Hourly data report for September 20, 2005: Pickle Lake A. Government of Canada, accessed 2 March 2022, https://climate.weather.gc.ca/climate_data/hourly_data_e.html?StationID=10251&timeframe=1&StartYear=1840&EndYear=2019&type=line&MeasTypeID=meantemp&wbdisable=true&time=LST&time=LST&Year=2005&Month=9&Day=20#.

Etkin, D., S. E. Brun, A. Shabbar, and P. Joe, 2001: Tornado climatology of Canada revisited: Tornado activity during different phases of ENSO. *Int. J. Climatol.*, **21**, 915–938, https://doi.org/10.1002/joc.654.

Gallus, W. A., Jr., N. A. Snook, and E. V. Johnson, 2008: Spring and summer severe weather reports over the Midwest as a function of convective mode: A preliminary study. *Wea. Forecasting*, **23**, 101–113, https://doi.org/10.1175/2007WAF2006120.1.

Grams, J. S., R. L. Thompson, D. V. Snively, J. A. Prentice, G. M. Hodges, and L. J. Reames, 2012: A climatology and comparison of parameters for significant tornado events in the United States. *Wea. Forecasting*, **27**, 106–123, https://doi.org/10.1175/WAF-D-11-00008.1.

Groenemeijer, P., and T. Kuhne, 2014: A climatology of tornadoes in Europe: Results from the European severe weather database. *Mon. Wea. Rev.*, **142**, 4775–4790, https://doi.org/10.1175/MWR-D-14-00107.1.

Hage, K. D., 1988: Tornado, a report: Edmonton and Strathcona County, July 31st, 1987. A History of Tornadoes in Alberta, Alberta Public Safety Services Rep., 196 pp., https://ia600207.us.archive.org/32/items/tornadoreportedm00albe_0/tornadoreportedm00albe_0.pdf.

——, 1994: Alberta tornadoes, other destructive windstorms, and lightning fatalities: 1879–1984. University of Alberta Tech Rep., 67 pp., ISBN 0-9696300-2-6, https://search.saskarchives.com/hage-keith-d-3.

Jedlovec, G. J., U. Nair, and S. L. Haines, 2006: Detection of storm damage tracks with EOS data. *Wea. Forecasting*, **21**, 249–267, https://doi.org/10.1175/WAF923.1.

King, P., 1997: On the absence of population bias in the tornado climatology of southwestern Ontario. *Wea. Forecasting*, **12**, 939–946, https://doi.org/10.1175/1520-0434(1997)012<0939:OTAOPB>2.0.CO;2.

Kingfield, D. M., and K. M. de Beurs, 2017: Landsat identification of tornado damage by land cover and an evaluation of damage recovery in forests. *J. Appl. Meteor. Climatol.*, **56**, 965–987, https://doi.org/10.1175/JAMC-D-16-0228.1.

Malamud, B. D., and D. L. Turcotte, 2012: Statistics of severe tornadoes and severe tornado outbreaks. *Atmos. Chem. Phys.*, **12**, 8459–8473, https://doi.org/10.5194/acp-12-8459-2012.

Marion, G. R., 2017: Controls of updraft size, cold pool characteristics, and potential tornado intensity in supercell thunderstorms. M.S. thesis, Dept. of Atmospheric Sciences, University of Illinois at Urbana–Champaign, 58 pp., https://www.ideals.illinois.edu/handle/2142/97792.

Molthan, A. L., J. R. Bell, T. A. Cole, and J. E. Burks, 2014: Satellite-based identification of tornado damage tracks from the 27 April 2011 severe weather outbreak. *J. Oper. Meteor.*, **2**, 191–208, https://doi.org/10.15191/nwajom.2014.0216.

Natural Resources Canada, 2020: 8 facts about Canada's boreal forests. Government of Canada, accessed 16 July 2020, https://www.nrcan.gc.ca/our-natural-resources/forests/sustainable-forest-management/boreal-forest/8-facts-about-canadas-boreal-forest/17394.

Newark, M. J., 1988: The tornado hazard in Canada. *Natural and Man-Made Hazards*, M. I. El-Sabh and T. S. Murty, Eds., Springer, 743–748.

Pisnichenko, I. A., 1994: The role of vapor-water phase transitions in the generation of tornadoes. *Izv. Atmos. Oceanic Phys.*, **29**, 761–765.

Planet, 2021: Visual basemaps. Developer Resource Center, accessed 15 December 2021, https://developers.planet.com/docs/data/visual-basemaps/.

Rodríguez, O., and J. Bech, 2020: Reanalysing strong-convective wind damage paths using high-resolution aerial images. *Nat. Hazards*, **104**, 1021–1038, https://doi.org/10.1007/s11069-020-04202-6.

Sayn-Wittgenstein, L., and J. M. Wightman, 1975: Landsat application in Canadian forestry. *Proc. 10th Int. Symp. on Remote Sensing of Environment*, Ann Arbor, MI, Environmental Research Institute of Michigan, 1209–1218, https://www.osti.gov/biblio/5116332.

Shikhov, A., and A. Chernokulsky, 2018: A satellite-derived climatology of unreported tornadoes in forested regions of northeast Europe. *Remote Sens. Environ.*, **204**, 553–567, https://doi.org/10.1016/j.rse.2017.10.002.

Sills, D. M. L., V. Cheng, P. J. McCarthy, B. Rousseau, J. Waller, L. Elliott, J. Klaassen, and H. Auld, 2012: Using tornado, lightning, and population data to identify tornado prone areas in Canada. *26th Conf. on Severe Local Storms*, Nashville, TN, Amer. Meteor. Soc., 59, https://ams.confex.com/ams/26SLS/webprogram/Manuscript/Paper211359/SLS26_manuscript_TornadoProne_FINAL.pdf.

——, and Coauthors, 2020: The Northern Tornadoes Project: Uncovering Canada's true tornado climatology. *Bull. Amer. Meteor. Soc.*, **101**, E2113–E2132, https://doi.org/10.1175/BAMS-D-20-0012.1.

——, C. S. Durfy, and C. P. E. de Souza, 2022: Are significant tornadoes occurring later in the year in southern Ontario? *Geophys. Res. Lett.*, **49**, e2021GL096483, https://doi.org/10.1029/2021GL096483.

Strong, W. L., and G. H. La Roie, 1983: Root-system morphology of common boreal forest trees in Alberta, Canada. *Can. J. For. Res.*, **13**, 1164–1173, https://doi.org/10.1139/x83-155.

Thompson, R. L., R. Edwards, J. A. Hart, K. L. Elmore, and P. Markowski, 2003: Close proximity soundings within supercell environments obtained from the Rapid Update Cycle. *Wea. Forecasting*, **18**, 1243–1261, https://doi.org/10.1175/1520-0434(2003)018<1243:CPSWSE>2.0.CO;2.

——, ——, and C. M. Mead, 2004: An update to the supercell composite and significant tornado parameters. *22nd Conf. on Severe Local Storms*, Hyannis, MA, Amer. Meteor. Soc., P8.1, https://ams.confex.com/ams/pdfpapers/82100.pdf.

——, C. M. Mead, and R. Edwards, 2007: Effective storm-relative helicity and bulk shear in supercell thunderstorm environments. *Wea. Forecasting*, **22**, 102–115, https://doi.org/10.1175/WAF969.1.

——, B. T. Smith, J. S. Grams, A. R. Dean, and C. Broyles, 2012: Convective modes for significant severe thunderstorms in the contiguous United States. Part II: Supercell and QLCS tornado environments. *Wea. Forecasting*, **27**, 1136–1154, https://doi.org/10.1175/WAF-D-11-00116.1.

Trapp, R. J., S. A. Tessendorf, E. S. Godfrey, and H. E. Brooks, 2005: Tornadoes from squall lines and bow echoes. Part I: Climatological distribution. *Wea. Forecasting*, **20**, 23–34, https://doi.org/10.1175/WAF-835.1.

——, G. R. Marion, and S. W. Nesbitt, 2017: The regulation of tornado intensity by updraft width. *J. Atmos. Sci.*, **74**, 4199–4211, https://doi.org/10.1175/JAS-D-16-0331.1.

Vahabi-Mashak, S., Z. Abdul-Malek, K. Mehranzamir, H. Nabipour-Afrouzi, B. Salimi, and C.-L. Wooi, 2015: Modeling of time of arrival method for lightning locating systems. *Adv. Meteor.*, **2015**, 870290, https://doi.org/10.1155/2015/870290.

Western University, 2021: Northern Tornadoes Project: Annual Report 2020. Western University Project Rep. 2, 66 pp., https://ir.lib.uwo.ca/ntp_reports/2.

Wurman, J., K. Kosiba, T. White, and P. Robinson, 2021: Supercell tornadoes are much stronger and wider than damage-based ratings indicate. *Proc. Natl. Acad. Sci. USA*, **118**, e2021535118, https://doi.org/10.1073/pnas.2021535118.

Yuan, M., M. Dickens-Micozzi, and M. A. Magsig, 2002: Analysis of tornado damage tracks from the 3 May tornado outbreak using multispectral satellite imagery. *Wea. Forecasting*, **17**, 382–398, https://doi.org/10.1175/1520-0434(2002)017<0382:AOTDTF>2.0.CO;2.